NDT&E International 147 (2024) 103215

Contents lists available at ScienceDirect

NDT and E International

journal homepage: www.elsevier.com/locate/ndteint

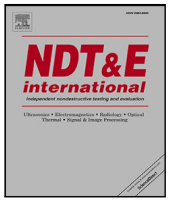

Research Paper

Ice matrix composites for Cryo-ultrasonic testing

Kaden C. Wells [a], Francesco Simonetti [a,*], Christian Peco [b], Andrea P. Argüelles [b]

[a] Department of Aerospace Engineering and Engineering Mechanics, University of Cincinnati, Cincinnati, 45221, OH, USA
[b] Department of Engineering Science and Mechanics, Penn State, University Park, 16802, PA, USA

ARTICLE INFO

Keywords:
Ultrasonic testing
Solid couplant
Alumina dispersions
Additive manufacturing

ABSTRACT

Cryo-ultrasonic testing utilizes polycrystalline ice coupling to enable the inspection of metallic components with complex shape. The relatively high velocity of compressional waves in ice (approximately 4000 m s^{-1}) and its ability to support the propagation of shear waves, significantly strengthen the ultrasonic transmission through curved interfaces over conventional water coupling. This paper explores the possibility of further enhancing the ultrasonic properties of ice by dispersing solid particles in water before it is frozen. Complex physicochemical phenomena occur when aqueous dispersions freeze which can lead to a solid material with microstructural characteristics that may be unfavorable to the propagation of ultrasonic waves. Here, these effects are controlled to produce a composite material consisting of alumina nanoparticles in an ice matrix. The composite exhibits compressional and shear wave velocities of approximately 4800 m s^{-1} and 2700 m s^{-1} , respectively. Importantly, the mass density of the material is more than twice as large as the density of water. Finally, it is shown that a phenomenon similar to a glass transition occurs during freezing which results in low ultrasonic attenuation when the temperature approaches – 100 °C.

1. Introduction

The ultrasonic inspection of metallic components with complex shape, such as those produced with additive manufacturing processes, poses several challenges when the inspection is conducted in immersion using water coupling. Due to the large contrast between the speed of compressional (P) waves in water (approximately 1500 m s^{-1}) and the velocity of P waves in metals (typically between 5500 m s^{-1} and 6500 m s^{-1}), it is necessary to orient the ultrasonic beam close to normal to the surface of the component. This is to prevent strong refraction effects that would otherwise cause excessive signal loss as the ultrasonic beam penetrates into the surface. Even at normal incidence, the strength of the signal entering the component is further limited by the mass density contrast between water and metals. Moreover, signal losses compound when the ultrasonic beam has to cross multiple water–metal interfaces as in the case of components with internal features such as channels and vanes. As a result, the industrial use of ultrasonic testing (UT) for the inspection of complex-shape components is currently rather limited.

Cryo-ultrasonic testing (Cryo-UT) has recently been proposed as a possible solution to expand the scope of UT applications. The underpinning idea is to replace the water couplant with polycrystalline ice and take advantage of its high P-wave velocity of nearly 4000 m s^{-1} and the fact that ice supports the propagation of shear (S) waves at approximately 2000 m s^{-1} [1]. In addition, ice has excellent adhesion properties to hydrophilic surfaces [2–4] or surfaces with some degree of roughness [5,6]. Therefore, P waves can be transmitted through an ice–metal interface for angles of incidence up to about 40 deg [1] which effectively eliminates the need for normal incidence transmission.

While ice provides a substantial improvement over water coupling, the mass density of ice (918 kg m^{-3}) is still low compared to metals and can affect the sensitivity of Cryo-UT. For instance, alternating layers of ice and metals, which occur when the internal features of a component are filled with ice, lead to wave reverberations between neighboring interfaces which pollute the waveforms and can cause artifacts when the signals are processed with image formation methods [7].

To further enhance the sensitivity of Cryo-UT, it is desirable to increase the mass density of ice as well as its ultrasonic velocities. Ideally, if it were possible to match the ultrasonic properties of the material of the component, the interfaces would become transparent to the incident wave and sensitivity to internal flaws would be maximized.

A possible strategy to control the mechanical properties of ice is to load its volume with a random distribution of solid particles leading to what can be regarded as a particulate reinforced composite. Using the rule of mixtures, the mass density of the composite material, ρ, can be expressed as $\rho = \rho_P\varphi + \rho_I(1-\varphi)$ where φ is the particle volume fraction and ρ_P and ρ_I are the mass densities of the particles and ice, respectively. If $\rho_P > \rho_I$ the density of the composite increases linearly

* Corresponding author.
E-mail address: f.simonetti@uc.edu (F. Simonetti).
URL: https://www.ase.uc.edu/USIL (F. Simonetti).

https://doi.org/10.1016/j.ndteint.2024.103215
Received 17 May 2024; Received in revised form 12 July 2024; Accepted 14 August 2024
Available online 17 August 2024

with φ. Therefore, utilizing composites with high density particles such as tungsten (approximately 19,300 kg m^{-3}) and with the appropriate volume fraction provide the possibility of matching the mass density of most metallic alloys of interest in engineering applications, typically below 9000 kg m^{-3}.

Predicting the effect that particles have on the ultrasonic velocities is less straightforward. There is not a universal model that applies to all types of particulate reinforced composites but rather a multitude of micromechanical models [8] whose validity depends on the specific mechanical properties of the matrix and particles as well as their volume fraction. Nevertheless, it can expected that particles will significantly increase the elastic moduli of ice leading to higher ultrasonic velocities as it is observed in the case of metal–matrix composites (e. g. Gür [9]).

Even more challenging is to predict the level of ultrasonic attenuation that the particles may induce. However, it can be observed that as long as the particles are much smaller than the ultrasonic wavelength and are perfectly bonded to the ice matrix, ultrasonic scattering by the particles will be negligible and so the resulting attenuation should be limited [10].

Since the ice composite has to embed the component to form a solid block, it is desirable to start from a liquid dispersion obtained by suspending the particles in water. The encapsulation process can then be performed in three consecutive steps: (1) Pour the dispersion into a mold containing the component; (2) Apply vacuum to degas the dispersion and remove air pockets from the component internal features; (3) Use directional freezing to solidify the dispersion as it is currently done with Cryo-UT [11]. After the block is inspected by scanning an ultrasonic probe over its surface, the component can be retrieved by simply melting away the composite material.

The encapsulation process rely on the feasibility of producing stable dispersions and ensuring that they yield the desired microstructure after freezing. These two aspects are discussed separately next.

1.1. Dispersion preparation

Aqueous dispersions of solid particles are widely used in the ceramic industry in a process known as slip casting. The dispersions are designed to maximize particle volume fraction while maintaining low viscosity which ensures that the dispersion can fill complex-shape molds; see, for instance, Tsetsekou et al. [12].

A key requirement in the preparation of these high concentration dispersions (slurries) is that the particles remain suspended in water with limited sedimentation. The stability of the slurries is governed by several physicochemical phenomena; some of which can be explained according to the Derjaguin, Landau, Verwey, and Overbeek (DLVO) theory [13]. For dispersions of small particles, Brownian motion of water molecules results in forces applied to the particles that are typically sufficient to counteract the effect of gravitational forces and maintain the dispersion stable even when the particle mass density is significantly higher than the density of water. However, if the particles aggregate, these forces may no longer be able to balance the weight of the aggregate.

Aggregation occurs because the Brownian motion can bring particles very close to each other. According to the DLVO theory, particles exchange attractive van der Waals forces and repulsive electrostatic forces that are the result of all particles having a net electric charge of the same sign. These forces increase as the distance between particles decreases and for aggregation to occur the attractive force must prevail on the repulsive one. The repulsive force is characterized through the so-called ζ-potential [14]. The higher the ζ-potential (in absolute value) the more stable the dispersion since more energy is required for bringing the particles close together.

The aggregation and sedimentation of particles can be prevented through the use of dispersants which produce either steric or electrostatic stabilization. The latter is performed by altering the electric charge of the particles and hence by increasing the ζ-potential. For aqueous dispersions, this can be achieved by controlling the pH of the dispersion. Several dispersants have been developed for the ceramic industry and a vast literature is available for the preparation of alumina (Al_2O_3) dispersions. Indeed, the stability achieved with alumina slurries [15–21] is remarkable given that the mass density of alumina (3965 kg m^{-3}) is about four times higher than that of water. The use of dispersants with appropriate dosage has also been shown to dramatically reduce viscosity [12,22].

1.2. Frozen dispersion microstructure

The microstructural properties of frozen aqueous dispersions have been the subject of extensive studies over the past twenty years due to the emergence of a new manufacturing technique named freeze casting. Here, dispersions are frozen to produce porous materials [23,24]. Much of this work is based on experimental observations that have highlighted a number of complex phenomena, many of which are not yet fully understood [23]. In this context, templating [25] is a key effect associated with the growth of ice crystals in water and which is used to arrange the particles in ordered lamellar structures. These consist of alternating layers of pure ice and particle-rich ice [26]. While templating is central to freeze casting, it is to be avoided in Cryo-UT applications as ordered structures can cause significant signal degradation due to scattering and anisotropy.

Templating is the result of the surface of an ice crystal pushing away the neighboring particles as the crystal grows. Whether particles are entrapped in the ice or rejected depends on the speed of propagation of the crystal boundaries. There exists a critical speed below which particles are rejected and which for diluted dispersions is inversely proportional to the particle radius and the liquid viscosity [27]. As a result, templating is more likely to occur at low freezing rates and for dispersions with low viscosity and small particles. The extent of templating is also dependent on the particle concentration. There exists a critical particle volume fraction called breakthrough concentration, φ_b, beyond which the particles are no longer rejected by the ice crystals [28,29]. φ_b decreases as the particle radius and the surface tension of the suspending medium decrease.

The ultrasonic properties of frozen dispersions can also be affected by the premelting phenomenon [30,31]. Premelting was originally observed in soils and is characterized by the presence of unfrozen water at temperatures well below its freezing point. In a frozen medium exhibiting premelting, only the interstitial spaces between particles are filled with ice while the individual particles are coated by a film of liquid water. The thickness of the film decreases with the degree of undercooling (difference between the melting temperature of ice and the temperature of the medium) and is dependent on a wide range of physical properties that include particle radius and concentration [32]. The effect of premelting on wave propagation has been studied in the context of frozen porous media [33–35]. These studies have indicated that the ultrasonic velocities decrease as the fraction of unfrozen water increases while the ultrasonic attenuation increases. As a result, premelting can have a negative impact on the ultrasonic properties of not fully frozen dispersions.

Finally, a significant unknown is whether the particles can compromise the adhesion strength of ice to metallic substrates. Poor adhesion could represent an impenetrable barrier to the ultrasonic signals especially at the highest inspection frequencies.

1.3. Aim of the present study

The main objective of this paper is to provide an initial assessment of the feasibility of using particle reinforced ice composites as ultrasonic couplant. The study encompasses four specific aims: (1) Establish a process to encapsulate a component in the ice composite; (2) Prove that it is possible to increase mass density and ultrasonic velocities

without causing excessive attenuation; (3) Demonstrate that particles do not compromise the strength of the bond to metallic surfaces; (4) Provide a scaled demonstration of the practicality of the proposed approach for Cryo-UT applications.

Section 2 presents the slurry preparation method and provides details about the encapsulation process and the design of a test cell to monitor the ultrasonic properties of the slurry as it freezes. After providing experimental results in Section 3, practical implications for Cryo-UT applications and the next steps for advancing the technology are discussed in Section 4. Finally, conclusions are given in Section 5.

2. Methods

2.1. Slurry preparation

The materials used for dispersion preparation were aluminum oxide Al_2O_3 alpha nanoparticles with 300 nm diameter (US Research Nanomaterials, Inc), deionized water, and ammonium polymethacrylate dispersant (Darvan C-N). Although other particles may be better suited for Cryo-UT applications, here Al_2O_3, which has mass density of 3965 $kg\,m^{-3}$, was selected to take advantage of the vast literature available about slurry preparation and stabilization as well as microstructural characterization after directional freezing.

The slurry was produced in small batches with volumes ranging from 0.2 L to 0.4 L. The process started by adding the dispersant to deionized water and stirring for 30 min. Subsequently, Al_2O_3 powder was gradually added to the water-dispersant solution under continuous sonication until a particle volume fraction $\varphi \approx 0.40$ was obtained, which corresponds to a mass density of about 2200 $kg\,m^{-3}$. This was below the breakthrough concentration $\varphi_b = 0.57$ required to prevent templating [29] and was the limit that could be achieved with the sonicator as buoyancy forces prevented the powder from sinking into the dispersions and particle aggregation began to occur. Moreover, as φ increases, sonication causes increasing levels of heat that lead to water evaporation and therefore requires periodic cooling of the dispersion. Multiple dispersions were prepared for different values of the dispersant to water mass ratio, ξ. Each time, a new batch of high purity (99.9%) alumina powder was used.

The preparation of the slurries was the limiting factor in this study as the sonication process could take up to 3 h and the powders were somewhat costly.

2.2. Experimental setup

The ultrasonic properties of the slurry were continuously monitored during the freezing process using the experimental apparatus shown in Fig. 1. The setup included a cylindrical mold consisting of a 25.4 mm thickness aluminum (alloy 7075) base and a 76.2 mm tall polytetrafluoroethylene (PTEF) wall. The wall had inner diameter of 76.2 mm and thickness of 38.1 mm to minimize heat conduction. The mold was cooled from the base by placing it in contact with an aluminum cold plate which was supported by an aluminum tower with legs immersed in liquid nitrogen. Heat elements mounted on the tower and connected to PID controllers were included to adjust the temperature of the cold plate.

The base of the mold was instrumented with a screw-in contact transducer placed at its center. Due to the presence of the transducer, the base could not be in direct contact with the cold plate and therefore an aluminum thermal shunt, with a cavity to accommodate the transducer, was positioned between the base and the cold plate.

An assembly consisting of two aluminum square blocks 50.8 × 50.8 mm^2 (thicknesses 12.7 mm and 22.2 mm) supported by three aluminum legs, Fig. 1(c), was placed inside the mold and bolted to the base. The block at the top (Block #2) was also instrumented with a screw-in contact transducer.

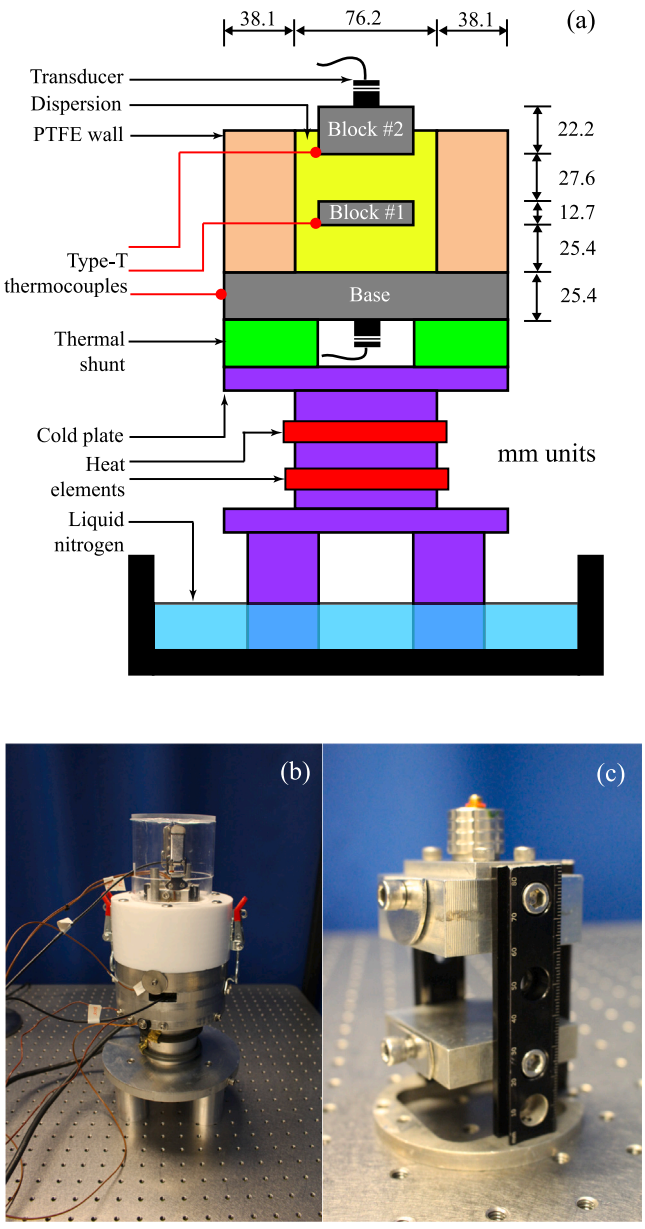

Fig. 1. (Color online). Apparatus used to monitor the ultrasonic properties of freezing dispersions. A mold formed by an aluminum base and a thick PTFE wall and containing an assembly consisting of two aluminum blocks is filled with the dispersion. The dispersion is directionally frozen by resting the mold on a cooling tower whose legs are immersed in liquid nitrogen. A pair of ultrasonic transducers is used to monitor the signals propagating through the dispersion and the aluminum blocks. (a) Diagram of the apparatus with selected dimensions provided in mm units; (b) Photograph of the test cell; (c) Detail of the block assembly mounted inside the mold.

Temperature was monitored by means of three, type-T thermocouples connected to the two blocks and to the base of the mold.

The mold was filled by pouring the liquid slurry from the top and with the block assembly in place. It was subsequently placed in a vacuum chamber until internal pressure reached about 10 Torr which was sufficient to cause the dispersion to boil. After releasing the vacuum, the mold was placed on the cold plate for directional freezing.

Most the of experiments were performed with a pair of compressional, 6 MHz (6 dB bandwidth from 4 MHz to 7.7 MHz), 12.7 mm diameter transducers (Cobra Scientific) and using glycol as the coupling agent. A smaller set of experiments was performed using a 3 MHz (6 dB bandwidth from 1.4 MHz to 4.1 MHz), 12.7 mm diameter shear transducer (Panametrics) mounted on the base and coupled with honey.

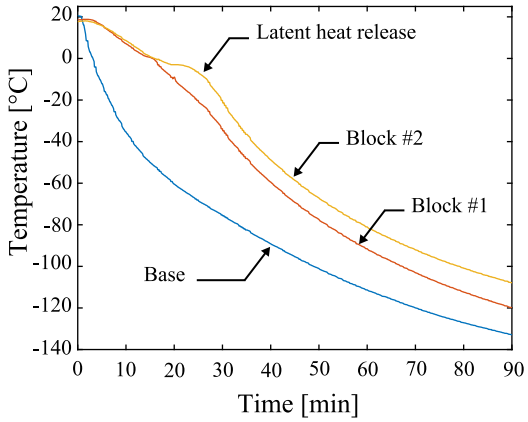

Fig. 2. (Color online). Temperature profiles measured by three Type-T thermocouples mounted on the base of the mold and the two blocks inside it during freezing of a $\varphi = 0.41$, $\xi = 0.15$ alumina dispersion.

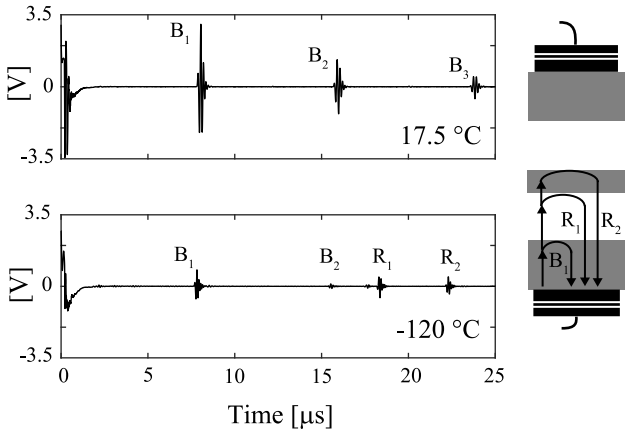

Fig. 3. Pulse-echo waveforms recorded with a 6 MHz compressional transducer mounted on the mold base and recorded when the temperature of Block #1 was 17.5 °C and −120 °C. The diagram shows the wave paths corresponding to the pulses indicated in the waveforms. Alumina dispersion with $\varphi = 0.41$ and $\xi = 0.15$.

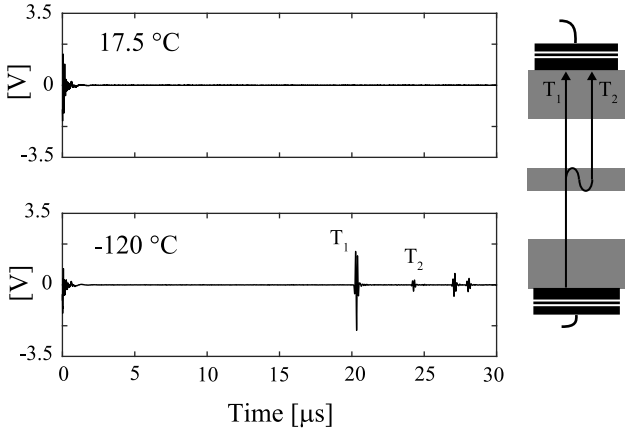

Fig. 4. Through-transmission waveforms recorded with a pair of 6 MHz compressional transducer at 17.5 °C and −120 °C. The diagram shows the wave paths corresponding to the pulses indicated in the waveforms. Alumina dispersion with $\varphi = 0.41$ and $\xi = 0.15$.

The transducers were driven by an Olympus pulser-receiver (5072RP) and the waveforms recorded at 10 s intervals with a Teledyne-LeCroy oscilloscope (Waverunner 606Zi) after ensemble average with 10 samples.

The smallest dispersion batches (0.2 L) partially filled the mold and only covered the bottom block (Block #1). For these tests, only pulse-echo measurements with the bottom transducer were performed. With the larger batches, measurements were performed by manually switching between pulse-echo and pitch-catch acquisition mode to record both reflection and through-transmission signals.

3. Results

This section first considers a single, $\varphi = 0.41$, alumina dispersion with dispersant-to-water mass ratio $\xi = 0.15$ to illustrate the fundamental trends that are observed during the freezing process. It then explores the effect that different ξ values have on the ultrasonic properties of the frozen dispersion.

3.1. General trends

Cooling of the dispersion begins from room temperature conditions and evolves according to the temperature ramps shown in Fig. 2. The large temperature gradient from the base to Block #2 is required to achieve a relatively high propagation speed for the freeze front and limit templating effects.

Initially, water enters a supercooled metastable state in which it remains in the liquid phase at temperatures below 0°C. Then suddenly, rapidly growing dentritic ice crystals branch into the bulk of the dispersion while leaving most of the water unfrozen. This stage is accompanied with the release of latent heat which causes the humps in the temperature profile of the two blocks seen in Fig. 2. The final stage is mediated by a freeze front that slowly propagates from the base to the top of the mold [36].

Fig. 3 compares the pulse-echo waveforms measured with the 6 MHz transducer at the base of the mold before and after solidification of the dispersion. The temperature is measured at the location of Block #1. At 17.5 °C, only the reflection from the first metal-dispersion interface, B_1, and its reverberations inside the thickness of the base plate (B_2 and B_3) are visible. The reflection from Block #1 is not detectable due to the high attenuation in the liquid dispersion. On the other hand, when the temperature reaches −120 °C the amplitude of B_1 decreases by more than 10 dB and the front and back reflections from Block #1, R_1 and R_2, become detectable. This is the combined effect of more energy entering the solid dispersion, due to its higher impedance, and less energy being dissipated as the signal travels through the medium. The corresponding signals measured in through transmission are shown in Fig. 4. Once again, the high attenuation in the liquid dispersion suppresses the propagation of the ultrasonic signal at 17.5 °C. On the other hand, after solidification, both the direct transmission, T_1, and its first reverberation, T_2, inside Block #1 can be detected. Importantly, the amplitude of T_1 is comparable to that of B_1 measured when the dispersion was liquid. This is remarkable because pulse T_1 is detected after propagating through four interfaces.

The amplitude trends of pulses B_1, R_1, and T_1 (measured considering the pulse envelope peak) throughout the freezing process are shown in Fig. 5. The amplitudes are plotted as a function of the temperature of Block #1 which approaches the average temperature across the dispersion at the later stages of the cooling process — the actual temperature bounds can be deduced from Fig. 2.

The amplitude of B_1 exhibits a sharp drop which occurs at around 16 °C (see arrow in Fig. 5). This corresponds to a base plate temperature of −12 °C and is associated with the initial formation of the freeze front on the surface of the plate. A similar effect is observed with pure water ice [11] and is due to the larger acoustic impedance of ice relative to water. The quasi linear amplitude decay observed below −20 °C is driven by the transducer response that weakens as temperature decreases — this was verified by monitoring B_1 as a function of temperature with an empty mold.

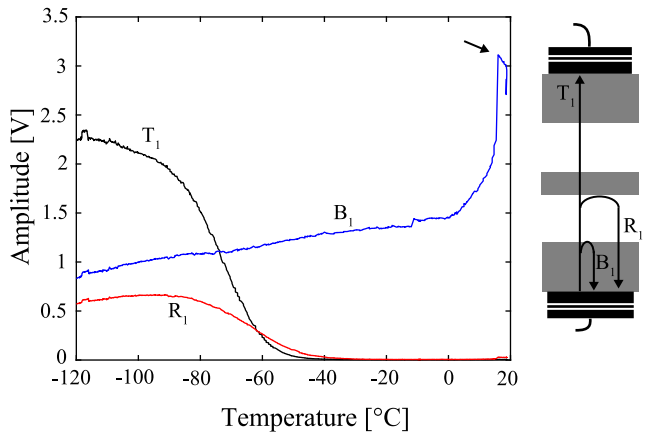

Fig. 5. (Color online) Ultrasonic monitoring of a freezing alumina dispersion with $\varphi = 0.41$ and $\xi = 0.15$ at 6 MHz. The amplitudes of the through-transmission signal, T_1, and the two reflected pulses B_1 and R_1 are shown as a function of the temperature of Block #1. The arrow indicates the onset of a freeze front on the surface of the base plate.

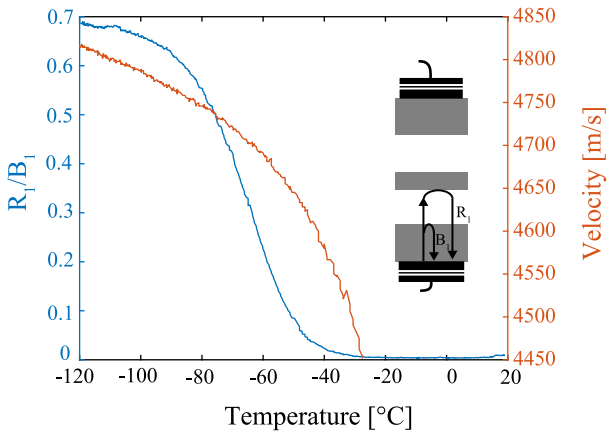

Fig. 6. (Color online) Normalized Block #1 reflection and compressional wave velocity of the dispersion as a function of temperature. Alumina dispersion with $\varphi = 0.41$ and $\xi = 0.15$.

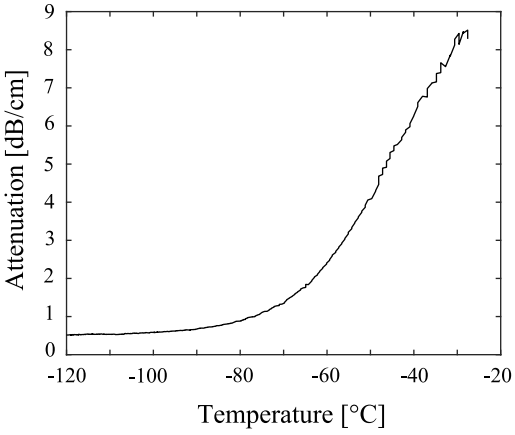

Fig. 7. Ultrasonic attenuation at 6 MHz as a function of temperature for an alumina dispersion with $\varphi = 0.41$ and $\xi = 0.15$.

Reflection R_1 becomes detectable when the temperature reaches about −40 °C and quickly grows as the temperature reaches −90 °C. Below this temperature, the amplitude decay is again due to the transducer response. The through-transmission pulse T_1 shows a similar trend as R_1.

The trends observed in Fig. 5 are reversible. As the temperature increases from −120 °C to room temperature, the amplitude moves along the same curves with very little hysteresis.

3.2. P-wave velocity

To eliminate the effect of the transducer temperature dependence, the amplitude ratio R_1/B_1 as a function of temperature is shown in Fig. 6. The figure also shows the speed of P waves in the dispersion estimated from the peak-to-peak traveltime difference between pulses R_1 and B_1. The values of velocity are not shown for temperatures above −28 °C since pulse R_1 was not detectable. The nonlinear temperature dependence observed as the temperature decreases down to −80 °C is consistent with the behavior of a partially frozen porous medium in which the fraction of unfrozen water decreases as the temperature decreases; thus, causing the velocity to increase [34]. For lower temperatures, the trend becomes linear as commonly observed with solid materials. At −120 °C, the velocity is 4818 $\mathrm{m\,s^{-1}}$ which is 25% higher than in pure water ice (3850 $\mathrm{m\,s^{-1}}$ at −10 °C).

3.3. P-wave attenuation

The data in Fig. 6 can be used to estimate an upper bound for the ultrasonic attenuation of P waves in the dispersion. Neglecting diffraction effects, assuming plane wave propagation, and defining the acoustic impedance of a medium as $Z = c\varrho$, where c is the ultrasonic velocity and ϱ the mass density, the ratio R_1/B_1 can be expressed as

$$\frac{R_1}{B_1} = \frac{4Z_aZ_d}{(Z_a+Z_d)^2}\exp(-2d\gamma), \tag{1}$$

where γ is the attenuation, d, the distance between the base plate and Block #1, and Z_a and Z_d are the acoustic impedances of aluminum and the dispersion, respectively. Solving for γ one obtains

$$\gamma = \frac{1}{2d}\ln\left[\frac{B_1}{R_1}\frac{4Z_aZ_d}{(Z_a+Z_d)^2}\right]. \tag{2}$$

In the first approximation, the effect of temperature on the mass density of aluminum and the dispersion are neglected and so the density of aluminum alloy 7075 at room temperature (2810 $\mathrm{kg\,m^{-3}}$) and the measured density of the liquid dispersion (2230 $\mathrm{kg\,m^{-3}}$) can be used to compute the impedances. The temperature dependence of the speed of sound in aluminum is accounted for by evaluating the actual velocity from the traveltime between pulses B_2 and B_1, see Fig. 3. The resulting ultrasonic attenuation as a function of temperature is shown in Fig. 7.

It should be stressed that the values in Fig. 7 are an overestimation of the attenuation due to the spreading of the ultrasonic beam. Because the propagation medium is multilayered and falls within the near field of the transducer, the classic Lommel diffraction correction [37] is inaccurate. A better approach is to evaluate the ratio R_1/B_1 using three-dimensional elastic wave simulations which account for the characteristics of the propagation medium and the transducer aperture. Due to the axial symmetry of the problem, the simulations can be performed based on the two-dimensional velocity-stress formulation of the wave equations provided in [38] which can be solved using a fully-explicit time domain finite difference scheme with staggered grid [39]. As an example, simulations performed using the parameters corresponding to the frozen dispersion at −120 °C yield $(R_1/B_1)_{\mathrm{num}} = 0.77$ which is slightly larger than the experimental value, $(R_1/B_1)_{\mathrm{exp}} = 0.68$, see Fig. 6. The attenuation can then be estimated as $\gamma = 20\log[(R_1/B_1)_{\mathrm{num}}/(R_1/B_1)_{\mathrm{exp}}]/2d = 0.21$ dB/cm which is about half the value reported in Fig. 7. Since the purpose of this paper is to assess the feasibility of ultrasonic coupling through frozen dispersions, rather than accurately characterizing the ultrasonic properties of a

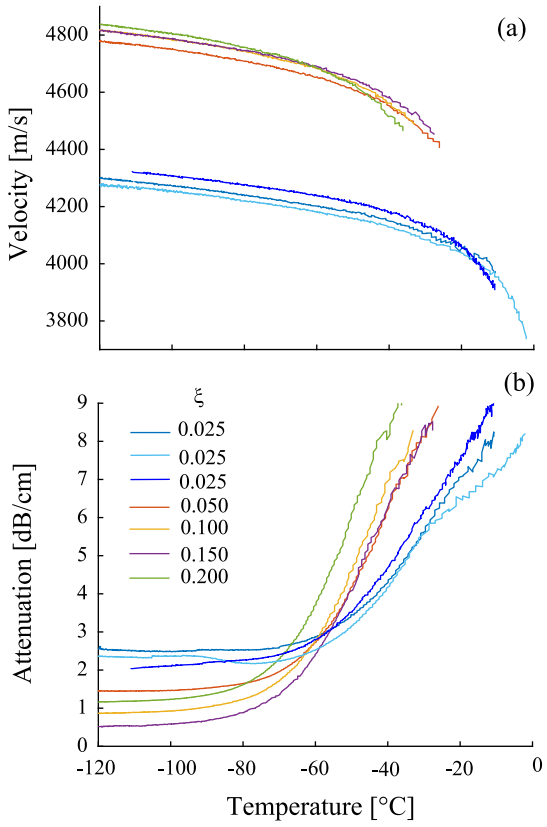

Fig. 8. (Color online) Effect of dispersant to water mass ratio, ξ, on the ultrasonic properties of alumina dispersions with constant volume fraction, $\varphi \approx 0.40$. (a) Compressional wave velocity; (b) Ultrasonic attenuation at 6 MHz.

specific type of dispersion, the diffraction correction will not be applied in the rest of this paper.

3.4. Effect of dispersant concentration

Comparison of the attenuation curve with the velocity plot in Fig. 6 reveals that when the attenuation stabilizes at around 0.5 dB/cm the velocity trend becomes linear suggesting that the solidification process may be completed between −80 °C and −100 °C. This is a much lower range than previously reported with calorimetry measurements (between −10 °C and −20 °C) [36] and is, at least in part, due to the use of a relatively high dispersant concentration.

To investigate the role played by the dispersant, Fig. 8 shows how the velocity and attenuation curves change as a function of ξ while the particle volume fraction is maintained constant at around 40%. The curves obtained for $\xi = 0.025$ correspond to an amount of dispersant equal to 1% of the mass of alumina powder used to make the dispersion. This is a common value used in freeze casting applications to minimize the viscosity of the dispersion. However, it consistently leads to the lowest ultrasonic velocity and the highest attenuation values — the three curves labeled as $\xi = 0.025$ refer to three different dispersion batches tested following the same experimental protocol to assess the repeatability of the results. At $\xi = 0.025$ the attenuation stabilizes at around −60 °C whereas for $\xi = 0.1$ or more the attenuation plateaus at about −80 °C.

Fig. 8, also shows that the P-wave velocity increases with ξ - a trend that was consistently observed by several other tests which are not reported in this paper. On the other hand, the ultrasonic attenuation seems to reach a minimum when $\xi = 0.15$. However, at this time it is not possible to exclude that this may be an artifact caused by the intrinsic variability of the frozen dispersion microstructure.

3.5. Glass-transition-like behavior

Some of the trends observed in Fig. 8 can be explained based on a phenomenon observed during the preservation of frozen foods and characterized by glass-transition temperatures similar to those reported in this paper [40]. In fact, the dispersant itself has a high solid percent (25% according to manufacturer). As temperature decreases and ice crystals grow in the water-dispersant solution, some of the solute is expelled from the crystals causing the concentration of the surrounding liquid solution to further increase. Increased concentration causes a depression in the freeze point of the solution which therefore remains liquid at increasingly lower temperatures. Additionally the presence of ice crystals in the solution increase its viscosity. This leads to a so-called freeze-concentrated state. At sufficiently low temperatures, the freeze-concentrated phase experiences a glass transition and takes the form of an amorphous glassy solid. Such a transition would most likely be accompanied with a drastic reduction in attenuation.

The dispersant could also play a critical role in preventing the templating phenomenon (i. e. the formation of lamellar structures). First, the viscosity of the dispersion increases with ξ [12] which inhibits the ability of the ice crystals to push the alumina particles. Moreover, it is possible that the solute in the dispersant may precipitate at the ice crystal boundary thus preventing the ice laminas from growing [41]. As a result, it is plausible that for $\xi = 0.025$ the frozen dispersion presents lamellar structures oriented in the vertical direction according to the freeze casting process. Such structures would certainly cause an increase in the ultrasonic attenuation and could also explain the lower ultrasonic velocity. On the other hand, for greater values of ξ the templating phenomenon may be significantly reduced leading to a frozen medium resembling a particulate reinforced composite with a random particle distribution.

3.6. S-wave properties

In closing this section, the shear properties of the ice composite are considered. The honey used to couple the transducer to the base of the mold tends to crack at around −100 °C (i. e. approximately −80 °C at Block #1) causing the transducer to disbond from the base. As a result, it was not possible to cover the same temperature range as it was done in the case of P waves. Fig. 9, shows the shear velocity and attenuation for a dispersion with $\varphi = 0.4$ and $\xi = 0.15$ as a function of the temperature of Block #1. The trends are similar to those observed with P waves. After solidification, the S-wave velocity approaches 2700 $m\,s^{-1}$ which is substantially higher than in pure water ice (1850 $m\,s^{-1}$ at −10 °C). The attenuation is much higher than that of P-waves but appears to stabilize in the same −80 °C to −100 °C range.

4. Discussion

4.1. Comparison with water coupling

The results presented in the previous section suggest that ultrasonic coupling with ice composites, formed by freezing alumina aqueous dispersions, offers several advantages over conventional water coupling. To illustrate them, through-transmission experiments were repeated by replacing the frozen dispersion with water at room temperature and maintaining all the other experimental parameters unchanged. The waveforms measured with water and the ice composite are shown in Fig. 10, from which three main observations can be made:

1. The through-transmission signal is much stronger with the composite. The amplitude of pulse T_1 through the composite is 16 dB above the corresponding value measured with water. The theoretical value obtained considering plane wave propagation is 21 dB. The difference can be ascribed to the attenuation in the composite, beam diffraction, and the fact that the transducer response is stronger at room temperature;

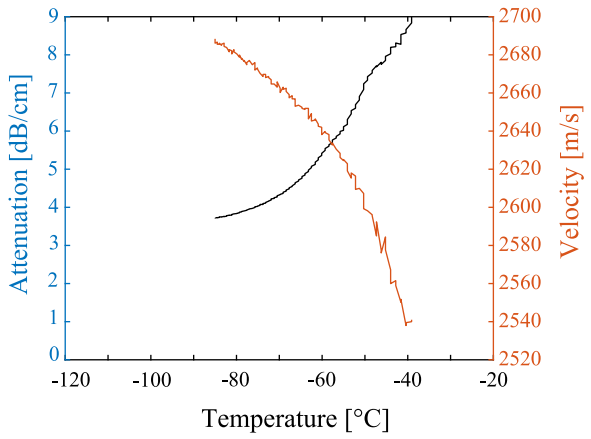

Fig. 9. (Color online) Ultrasonic shear velocity and attenuation at 3 MHz for an alumina dispersion with $\varphi = 0.40$ and $\xi = 0.15$.

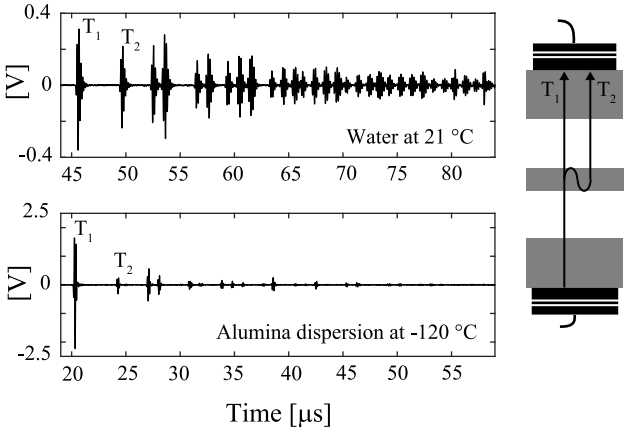

Fig. 10. Comparison between the through-transmission signals measured through water and the frozen alumina dispersion ($\varphi = 0.40$ and $\xi = 0.15$) at 6 MHz, all settings being the same. The waveforms are shown over a 40 μs time window but with different vertical scales.

2. The alumina particles do not appear to degrade the adhesion of the composite to the metallic substrate. The relatively high frequency of pulse T_1 and the fact that it crosses four interfaces imply that imperfect bonding would lead to severe amplitude losses. This is inconsistent with the large amplitude of T_1;
3. When the pulse travels through water, the large water–aluminum impedance mismatch causes significant internal reverberation resulting in multiple wave pulses that pollute the waveform. With the composite this effect is much reduced. If there were perfect impedance matching between aluminum and the composite, the waveform would only contain pulse T_1.

The example provided in Fig. 10 is limited to a normal incidence configuration. However, the major benefit of ultrasonic coupling through ice composites manifests at oblique incidence and is most apparent in the presence of heavy alloys such as Inconel. Fig. 11 considers transmission through a planar interface formed between a frozen alumina dispersion and Inconel and the corresponding case in which water coupling is used. The power transmitted through the interface is given as a function of the angle, α, formed between the incident wave (of unit power) and the normal to the interface. In both cases, the incident wave is a P wave and the transmitted power is carried by a P wave and a mode converted S wave until the angle of incidence reaches the critical value $\alpha^{cr}_{P,S}$ beyond which the relevant wave mode becomes evanescent. The critical angles are expressed as $\alpha^{cr}_{P,S} = \arcsin(a/c_{P,S})$

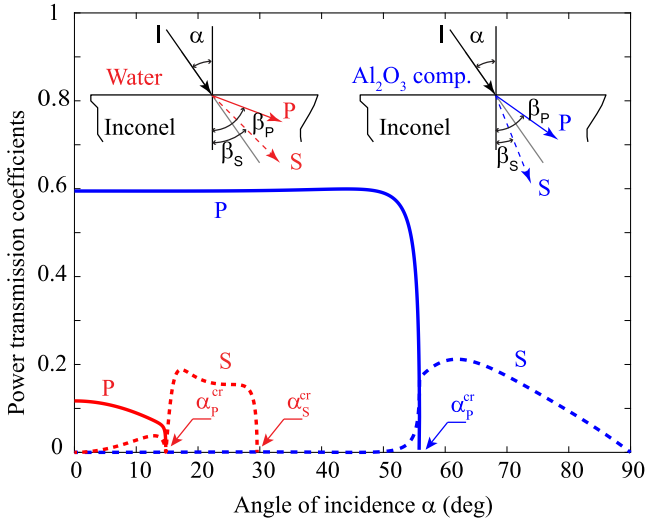

Fig. 11. (Color online) Ultrasonic power transmission into an Inconel half space through water (red) and Al_2O_3-ice composite at −120 °C (blue) coupling. The incident field is a compressional (P) wave whose propagation direction forms an angle α with the normal to the aluminum surface. The transmitted wavefield consists of a plane P-wave (solid curve) refracted at angle β_P and a mode converted shear (S) wave (dashed curve) propagating at angle β_S. The angles $\alpha^{cr}_{P,S}$ mark the critical incidences beyond which the transmitted wave mode becomes evanescent. With composite ice coupling transmission is possible at all angles while, with water, power cannot be transmitted beyond $\alpha^{cr}_S = 30°$.

Table 1
Ultrasonic velocities and densities used to predict power transmission coefficients.

Materials	P-wave vel. ($m\,s^{-1}$)	S-wave vel. ($m\,s^{-1}$)	Density ($kg\,m^{-3}$)
Water	1480	NA	1000
Al_2O_3 composite (−120 °C)	4800	2700	2200
Inconel	5800	3000	8200

where a is the speed of P waves in the coupling medium (water or ice composite) and c_P and c_S are the velocities of P and S waves in Inconel, respectively. The curves are obtained using the standard elastodynamic theory of plane wave scattering by interfaces [42] assuming that all the media are isotropic and homogeneous (material properties are listed in Table 1) and that the media are perfectly bonded at the interface to ensure continuity of displacement and stress.

With the ice composite, P-wave transmission is possible for a broad range of angles up to 55 deg. Moreover, the transmitted power is nearly constant within this range and contrasts the rapid decay that is observed in immersion. As in the case of pure water ice coupling, the mode converted S wave offers the possibility of achieving transmission for any other angle of incidence above 55 deg.

The ability to transmit the ultrasonic beam at large angles of incidence is critical to the inspection of complex-shape components which often present highly curved boundaries. With ice composites it may be possible to further extend the range over which P-wave transmission occurs by designing new dispersions which minimize the P-wave velocity contrast with the material of the component. This would also minimize refraction effects which are known to affect the sensitivity of ultrasonic imaging methods when applied to solids with doubly curved boundaries [43,44]. In this context, it should be emphasized that powder technologies have been developed to serve a broad range of industries including food, pharmaceutical, manufacturing, and metal processing. As a result, particles are produced with a variety of materials and are available in a wide range of sizes. This provides a high degree of flexibility when designing new dispersions.

4.2. Practical considerations

From a practical perspective, the process of encapsulating a component in an ice composite appears to be viable even in the presence of highly complex geometries. The limited space inside the mold and the structure of the block assembly shown in Fig. 1(c) provide a good example of what can be considered as an *hard-to-fill* geometry. The high fluidity of the dispersion in combination with the application of vacuum provide a robust solution to ensure that all spaces are filled by the dispersion.

After the ultrasonic inspection is completed, the ice composite is removed from the component by applying heat to the base of the mold and washing away the melted dispersion. To recover the alumina powder, the dispersion is first dried to remove the water and the solvent of the dispersant. After the liquid phase evaporates, the particles aggregate to form a solid similar to dried mud. The powder form is restored by grinding the material in a blender. Experiments (not reported in this paper) show that the ultrasonic properties of frozen dispersions obtained with recycled particles are comparable to those measured with fresh powder batches. However, as the same powder is reused multiple times the residual from the dispersant increases and in some cases leads to high ξ values which can result in excessive slurry viscosity.

The main limitation of the current process is the use of sonication to mix the dispersions; it is time consuming and yields low throughput. More effective would be the use of ball milling which is the standard method employed in the ceramic industry to make slurries in large volumes. Moreover, this technique is better suited to produce higher volume fractions beyond the breakthrough concentration [45].

Finally, an important challenge is represented by the need for performing the ultrasonic inspection at temperatures in the order of −100 °C. Currently, Cryo-UT is performed by scanning an ultrasonic probe on the surface of the ice block using a computer-controlled motion system housed in a cold room at −10 °C. One possibility, is to continue to use a room at −10 °C and only cool the specimen to −100 °C using a setup similar to that shown in Fig. 1. A prototype system to test this solution is currently under construction. The ultrasonic P-wave transducers used in this study are already ruggedized to work at such low temperature.

5. Conclusions

The possibility of using particle reinforced ice as an ultrasonic couplant is attractive for the inspection of complex-shape metallic components. To be practically applicable, the ice composite should be formed by freezing a liquid aqueous dispersion of particles. In this way, the component can be immersed in the liquid dispersion and subsequently subject to directional freezing to form a solid block.

Ice reinforced with alumina nanoparticles (40% vol.) exhibits compressional (P) and shear (S) wave velocities that are in the order of 4800 $\mathrm{m\,s^{-1}}$ and 2700 $\mathrm{m\,s^{-1}}$, respectively. Moreover, the mass density of the composite is around 2200 $\mathrm{kg\,m^{-3}}$. The composite is obtained from aqueous dispersion stabilized with ammonium polymethacrylate dispersant which prevents particle sedimentation.

The dispersant concentration plays a critical role during the solidification of the dispersion determining the temperature range at which the liquid-to-solid transition occurs as well as affecting the microstructure of the frozen dispersion. At low dispersant concentration, ordered lamellar structures can form that are detrimental to the ultrasonic properties. To prevent them it is necessary to use a dispersant-to-water mass ratio of about 10% or higher. The solidification of the dispersion appears to be mediated by a phenomenon similar to a glass transition which is completed at temperatures approaching −100 °C.

While the liquid dispersion is highly attenuative, the fully frozen ice composite shows relatively low attenuation, under 0.5 dB/cm at 6 MHz for P waves.

When compared to conventional water coupling, the superior ultrasonic properties of the ice composite lead to stronger transmission through multiple metallic interfaces and drastically reduce multiple scattering effects.

While this paper has focused on alumina nanoparticles, many different materials are available in powder form and over a wide range of particle diameters. Therefore, it may be possible to produce new ice composites that result in even greater mass density and ultrasonic velocities. Ideally, the properties of the composite could be tuned to match the ultrasonic properties of different metallic alloys.

CRediT authorship contribution statement

Kaden C. Wells: Writing – original draft, Visualization, Software, Formal analysis. **Francesco Simonetti:** Writing – review & editing, Software, Funding acquisition, Formal analysis, Conceptualization. **Christian Peco:** Writing – review & editing, Funding acquisition, Formal analysis, Conceptualization. **Andrea P. Argüelles:** Writing – review & editing, Funding acquisition, Formal analysis, Conceptualization.

Declaration of competing interest

The authors declare the following financial interests/personal relationships which may be considered as potential competing interests: Dr. Francesco Simonetti is affiliated to Cobra Scientific; a private company operating in the field of nondestructive testing If there are other authors, they declare that they have no known competing financial interests or personal relationships that could have appeared to influence the work reported in this paper.

Data availability

Data will be made available on request.

Acknowledgments

This material is based upon work supported by the National Science Foundation, USA under Grant No. 202911. Any opinions, findings, and conclusions or recommendations expressed in this material are those of the authors and do not necessarily reflect the views of the National Science Foundation.

References

[1] Simonetti F, Uchic M. Equiaxed polycrystalline ice for ultrasonic testing of solids. Phys Rev Appl 2022;18:014034.
[2] Raraty L, Tabor D. The adhesion and strength properties of ice. Proc R Soc Lond Ser A 1958;18:4–201.
[3] Archer P, Gupta V. Measurement and control of ice adhesion to aluminum 6061 alloy. J Mech Phys Solids 1998;46:1745–71.
[4] Matsumoto K, Kobayashi T. Fundamental study on adhesion of ice to cooling solid surface. Int J Refrig 2007;30:851–60.
[5] Zou M, Beckford S, Wei R, Ellis C, Hatton G, Miller M. Effects of surface roughness and energy on ice adhesion strength. Appl Surf Sci 2011;257:3786–92.
[6] Li R, Alizadeh A, Shang W. Adhesion of liquid droplets to rough surfaces. Phys Rev E 2010;82:041608.
[7] Simonetti F. Cryo-ultrasonic testing of curved components. NDT E Int 2023;137:102835.
[8] Jagadeesh G, Gangi Setti S. A review on micromechanical methods for evaluation of mechanical behavior of particulate reinforced metal matrix composites. J Mater Sci 2020;55:9848–82.
[9] Gür C. Investigation of microstructure–ultrasonic velocity relationship in sicp-reinforced aluminium metal matrix composites. Mater Sci Eng A 2003;361:29–35.
[10] Biwa S, Watanabe Y, Motogi S, Ohno N. Analysis of ultrasonic attenuation in particle-reinforced plastics by a differential scheme. Ultrasonics 2004;43:5–12.
[11] Simonetti F, Fox M. Experimental methods for ultrasonic testing of complex-shaped parts encased in ice. NDT E Int 2019;103:1–11.

[12] Tsetsekou A, Agrafiotis C, Milias A. Optimization of the rheological properties of alumina slurries for ceramic processing applications part i: Slip-casting. J Eur Ceram Soc 2001;21:363–73.
[13] Guozhong C. Nanostructures and nanomaterials: synthesis, properties and applications. World scientific; 2004.
[14] Hunter R. Zeta potential in colloid science: principles and applications, vol. 2, Academic Press; 2013.
[15] Davies J, Binner J. The role of ammonium polyacrylate in dispersing concentrated alumina suspensions. J Eur Ceram Soc 2000;20:1539–53.
[16] Palmqvist L, Lyckfeldt O, Carlström E, Davoust P, Kauppi A, Holmberg K. Dispersion mechanisms in aqueous alumina suspensions at high solids loadings. Colloids Surf A 2006;274:100–9.
[17] Gaydardzhiev S, Ay P. Characterisation of aqueous suspensions of fumed aluminium oxide in presence of two dolapix dispersants. J Mater Sci 2006;41:5257–62.
[18] Singh B, Bhattacharjee S, Besra L, Sengupta D. Electrokinetic and adsorption studies of alumina suspensions using darvan c as dispersant. J Colloid Interface Sci 2005;289:592–6.
[19] Kim D, Kim H, Lee J. Dependence of the rheological behaviour of electrostatically stabilized alumina slurries on ph and solid loading. J Mater Sci 1998;33:2931–5.
[20] Singh B, Bhattacharjee S, Besra L, Sengupta D. Evaluation of dispersibility of aqueous alumina suspension in presence of darvan c. Ceram Int 2004;30:939–46.
[21] Lu K, Kessler C, Davis R. Optimization of a nanoparticle suspension for freeze casting. J Am Ceram Soc 2006;89:2459–65.
[22] Chou K, Lee L. Effect of dispersants on the rheological properties and slip casting of concentrated alumina slurry. J Am Ceram Soc 1989;72:1622–7.
[23] Scotti K, Dunand D. Freeze casting–a review of processing, microstructure and properties via the open data repository, freezecasting.net. Prog Mater Sci 2018;94:243–305.
[24] Deville S. Freezing colloids: observations, principles, control, and use: applications in materials science, life science, earth science, food science, and engineering. Springer; 2017.
[25] Deville S. Ice-templating, freeze casting: Beyond materials processing. J Mater Res 2013;28:2202–19.
[26] Deville S, Saiz E, Tomsia A. Ice-templated porous alumina structures. Acta Mater 2007;55:1965–74.
[27] Körber C, Rau G, Cosman M, Cravalho E. Interaction of particles and a moving ice-liquid interface. J Cryst Growth 1985;72:649–62.
[28] Deville S, Bernard-Granger G. Influence of surface tension, osmotic pressure and pores morphology on the densification of ice-templated ceramics. J Eur Ceram Soc 2011;31:983–7.
[29] Shanti N, Araki K, Halloran J. Particle redistribution during dendritic solidification of particle suspensions. J Am Ceram Soc 2006;89:2444–7.
[30] Cahn J, Dash J, Fu H. Theory of ice premelting in monosized powders. J Cryst Growth 1992;123:101–8.
[31] Dash J, Rempel A, Wettlaufer J. The physics of premelted ice and its geophysical consequences. Rev Modern Phys 2006;78(695).
[32] Hansen-Goos H, Wettlaufer J. Theory of ice premelting in porous media. Phys Rev E 2010;81:031604.
[33] Leclaire P, Cohen-Tenoudji F, Aguirre-Puente J. Extension of Biot's theory of wave propagation to frozen porous media. J Acoust Soc Am 1994;96:3753–68.
[34] Carcione J, Santos J, Ravazzoli C, Helle H. Wave simulation in partially frozen porous media with fractal freezing conditions. J Appl Phys 2003;94:7839–47.
[35] Matsushima J, Suzuki M, Kato Y, Rokugawa S. Ultrasonic measurements of attenuation and velocity of compressional and shear waves in partially frozen unconsolidated sediment and synthetic porous rock. Geophysics 2016;81:D141–53.
[36] Lasalle A, Guizard C, Leloup J, Deville S, Maire E, Bogner A, Gauthier C, Adrien J, Courtois L. Ice-templating of alumina suspensions: effect of supercooling and crystal growth during the initial freezing regime. J Am Ceram Soc 2012;95:799–804.
[37] Sedov A, Schmerr Jr L. Elastodynamic diffraction correction integrals. J Acoust Soc Am 1989;86:2000–6.
[38] Liu Q. Perfectly matched layers for elastic waves in cylindrical and spherical coordinates. J Acoust Soc Am 1999;105:2075–84.
[39] Preston L. Nonlinear to linear elastic code coupling in 2-d axisymmetric media. Technical report, Albuquerque, NM (United States): Sandia National Lab.(SNL-NM); 2017.
[40] Zhao J, Kumar P, Sablani S. Glass transitions in frozen systems as influenced by molecular weight of food components. Compr Rev Food Sci Food Saf 2022;21:4683–715.
[41] Wu S, Zhu C, He Z, Xue H, Fan Q, Song Y, Francisco J, Zeng X, Wang J. Ion-specific ice recrystallization provides a facile approach for the fabrication of porous materials. Nature Commun 2017;8(15154).
[42] Achenbach J. Wave propagation in elastic solids, vol. 16, Elsevier; 2012.
[43] McKee J, Bevan R, Wilcox P, Malkin R. Volumetric imaging through a doubly-curved surface using a 2d phased array. NDT E Int 2020;113:102260.
[44] Cosarinsky G, Cruza J, Muñoz M, Camacho J. Automatic estimation of surface and probe location for 3d imaging with bidimensional arrays. NDT E Int 2024;141:102990.
[45] Tong J, Chen D. Preparation of alumina by aqueous gelcasting. Ceram Int 2004;30:2061–6.